Estimation of Magnetic Fields in Direct-Drive Implosions

Stefan Astheimer

Estimation of Magnetic Fields in Direct Drive Implosions

By Stefan Astheimer

TABLE OF CONTENTS

Abstract

Charged particles are used to infer the extent of compression in implosions on OMEGA. Statistically significant variances in particle yield have been observed at different locations around the target. These variations are unexpected because the fusion reaction that produces the charged particles is isotropic. One possible cause for this deviation could be the existence of magnetic fields in the target. Magnetic fields can result from hydrodynamic instabilities in the implosion. Large fields would be able to bend the trajectories of charged particles significantly, possibly causing this variation in the particle yield. Using results from a two-dimensional hydrodynamic simulation of an implosion, the magnetic field source term and resulting deflection of charged particles have been estimated. The estimated strength of the magnetic field should be regarded as an upper limit as it does not include effects of return currents etc. The calculated deflection is small, but not irrelevant when compared with the slit size of the measurement devices. This suggests that magnetic fields cannot be ruled out as a possible cause for the variation in charged particle yields.

1. Introduction

Direct drive fusion implosions are a very important field of research in today's scientific community. They may hold the keys to unlimited power supply and also offer a laboratory for the study of astrophysical phenomena. Thus, it is important that we understand all that we can about these implosions. Scientists use the distribution of charged particles produced in the fuel core to infer about compression. Since particle production is isotropic, scientists expect a very even distribution of particle yield with

respect to placement of the detector. This should be true even if there are nonuniformities in the target. However, instead, scientists find a distribution that varies greatly in places (see Figure 1). In fact, there is deviation by as much as a factor of two between detectors. There are a variety of possible reasons for this unusual distribution; one possible cause is the presence of magnetic fields, which can be created internally in direct drive implosions.

Density and temperature gradients in inertial confinement fusion implosions result in hydrodynamic instabilities. These instabilities result in non-collinear gradients in the density of charge and electron temperature around the fuel shell and ablation surface of the implosion. These gradients lead to the formation of magnetic fields at the surfaces. These fields can cause particles, even the most energetic, to change trajectories, and deflect as they pass through the field. To determine whether or not internally created magnetic fields are actually responsible for the altered variance, we used a DRACO hydrocode simulation to estimate the magnitude of the fields and the resultant deflection of charged particles. In section II, we will describe the simulation. Section III describes the steps involved in the calculation of the magnetic field. Section IV discusses the results in the context of particle trajectories, and we conclude in section V.

2. About the DRACO Simulation

DRACO is a two dimensional hydrocode that models the conditions of an implosion, similar to those at the LLE. In the simulation considered, DRACO takes into account nonuniformities in the laser. It should be noted that the magnetic field computations we have performed are post-processing computations. Had the magnetic field computations been placed inside of the actual simulation, there would need to be

adjustment for back-current and convection which are formed by the movement of plasma, and which partially counteract the effects of the magnetic fields. Thus, what is estimated is an upper limit on the magnitudes of the magnetic fields.

Background

Nonuniformities in the incident laser light are imprinted on the plastic shell of the core. These imprinted perturbations grow during the ablation phase. Furthermore, through a process known as feedthrough, these perturbations travel through the plastic shell and are imprinted on the fuel surface. During the compression phase, these perturbations grow as Rayleigh-Taylor instabilities, and can give rise to the magnetic fields during the time of peak particle production.

In the absence of fields, since particle production is isotropic, the particles should be evenly incident on different placements of the detector. However, if the magnetic field is significant and nonuniform enough, the trajectories will be altered, and the particles will deflect, leading to an altered distribution.

3. Computational Processes

NonCollinear Gradient Computation

Maxwell's laws were used to compute the strength of the magnetic fields. Maxwell's laws express magnetic field strength as the cross product of the gradients of electron density and temperature (see appendix A). We therefore compute the gradients of electron density and temperature in order to compute the magnitude of the magnetic fields at the time of peak particle production. Figures 2 through 5 show contour plots of

charge density and cell temperature, as well as vector diagrams of their respective gradients. The gradients are computed numerically from the values of a given cell and its neighbors, and the distances between cells. Because the gradients are computed using the neighboring cells, the gradients of the innermost and outermost cells are not calculated. However, by looking at the contour plots of electron density and temperature, it is clear that the values near the origin and very far from the center are very uniform. Thus, the magnetic fields at these places are so trivial as to be irrelevant to further computations.

Curl Calculation

Figure 6 depicts the values of the partial time derivative of the magnetic field at the time of 1.9 ns, which is the time of peak particle production. The values of this partial derivative were computed using the Maxwell equations for magnetic fields. The time derivative is expressed as a function of the cross product of the gradients of electron density and cell temperature at the time step. Notice that there are two places where the derivative is exceptionally high. The closer of the two, located approximately 35 microns from the center, is the fuel shell interface; the farther away of the two is from residual gradients arising from instabilities in the ablation surface earlier in the implosion during the acceleration phase. Finally, notice that the derivative takes both positive and negative values. This shows that the magnetic field assumes both positive and negative directions.

Field Calculation

Figure 7 shows the magnitude of the magnetic field's strength after the implosion has gone on for 1.9 nanoseconds. This time step is of particular interest because this is

the time at which particle production is greatest. Unfortunately, the simulation records its output only once every 20 picoseconds, and the fuel cell surface of the target traverses a distance of almost 4 microns in the 20 picoseconds between measurements at 1.88ns and 1.9 ns, thus, it is almost impossible to create an accurate time integral over even such a small period of time. Instead, the magnetic field strength was computed by multiplying the interpolated values of the field strength gradient by the time interval of 30 picoseconds to obtain an approximate integral value. This time interval was computed by dividing the approximate length of the significant fields (10 microns) by the velocity at which the fluid moves (about 30,000,000 cm/s). This gives a timescale for which the motion of the field is, more or less, reasonable (Appendix A). The magnetic field is greatest, the order of 1 to 10 MegaGauss, at a distance of about 35 microns from the center of the target. The magnitude of the earth's magnetic field is approximately one quarter of a Gauss, and the largest fields ever created in a lab setting are on the order of 1-10 KiloGauss, which is about one thousand times less potent than the implosion's fields. Clearly the magnetic fields in these implosions are immensely powerful. Recall that this distance almost exactly correlates to the boundary of the fuel-shell surface. These instabilities have created noncollinear temperature and density gradients that resulted in the formation of the magnetic field. There is also a smaller field at about 70 microns out, which is a remnant from earlier instabilities that were created at the boundary of the ablation surface during the early parts of the implosion. At all other places, the magnetic fields are only on the order of a few gauss, and thus comparatively negligible. Notice the width of the band of high field strength at the fuel shell interface. It is on the order of 2 to 10 microns, however, it is generally only 2 to 4 microns wide.

Length Scale Calculations

Figures 8 and 9 show the computed scale length with respect to both electron density and cell temperature at the time of peak particle production. These lengths were computed by taking the values of electron density and cell temperature and dividing them by the norms of their respective gradients. The figures show that these fields have lengths of between 2 and 10 microns. Notice that the temperature length scales at the fuel shell surface are much greater than density length scales. This is because at the fuel shell interface, the electron density changes drastically across a very small distance, however, as we have seen in Figures 2 through 5, the temperature changes gradually across a relatively large distance.

4. Results

Trajectory Bend Calculations

Figures 10 and 11 depict the amount of bending that 14.5 MeV protons and 10 MeV deuterons experience as they pass through magnetic fields of varying strength and width. These particles are of interest as they are used to infer compression in fusion implosions. The values for these were computed outside the simulation and the postprocessing code. The Larmor radius and the magnitude of the field were calculated from the postprocessing data, and plotted separately to determine an approximate range of deflection values. The angles by which the particles were deflected were on the order of one tenth of a degree, or one six-hundredth of a radian. Notice that the amount of deflection varies more or less hyperbolically with changes in either field strength or scale length. Also observe that fields of strength of one or more MegaGauss require a

relatively small scale to alter the trajectory of these highly energetic protons and deuterons. These relevant magnitudes are present near the fuel shell interface. In a number of places, the particles may be subjected to such fields for distances of five to ten microns if they are deflected back into the field. These distances are more than enough to cause some very energetic particles like the protons and deuterons to deflect by as much as a third to a half of a millimeter as they travel the distance, about 20 centimeters, between their egress from the significant magnetic fields and their incidence upon the detector. This deflection is significant when compared to the slit width of the detector, so although the angles of deflection are tiny, the distance the particles travel, 20 cm, is large enough compared to the detector's slit width to lead to significant deflection.

Other Possible Issues

Internally created magnetic fields may not be the only things to alter the trajectories of charged particles. The most obvious explanation for the varied distribution may be related to the detectors themselves. One possible error may be a lack of cross calibration. However, the producers of the spectrometer which was used as a detector are reasonably sure that no such faults exist in their devices. Thus, we will not consider the experimental apparatus as a source for such large errors. There are a number of other possible properties of the implosion that may also play a role. First, it has been hypothesized that there exist external magnetic fields that are formed during the implosion. These externally created magnetic fields may have some impact on the paths of the particles, but we have no estimate of their size, and it seems very unlikely that, without the massive gradients of electron density and temperature present at the fuel shell interface, the external fields are large enough to bend the trajectories significantly.

(Recall that the magnetic fields at the fuel shell interface during the time of peak particle production are on the order of a thousand times greater than any ever created in a controlled environment.) Second, it is possible that the laser itself influences the motion of the particles. However, since the laser has been turned off almost one whole nanosecond before the time of peak particle production, the magnitudes of the magnetic fields intrinsic to the laser beams may have decayed to irrelevant trace levels. Thus, the lasers themselves may have little if any effect on the trajectories, especially those of such energetic charged particles. Finally, it is possible that particle production is actually anisotropic with respect to angle. Plasma properties, such as a polarization of the spin of the fusing ions, may result in nonuniformities in particle production. If this were the case the distribution of energetic, charged particles would not be uniform, regardless of the presence of magnetic fields. However, there have been many tests done, showing that the processes involved in the particle production in lower temperature laboratory situations are isotropic. It is logical to extend this generalization to high temperatures and densities. In doing so, we can assume that the contribution from spin polarization is small.

5. Conclusions

It should be noted that the hydrodynamic properties of the plasma are not affected by the magnetic fields very much. The absolute maximum pressure exerted by the magnetic fields is on the order of one million atmospheres, approximately two orders of magnitude lower than the minimum value of the intrinsically created pressure of the plasma. Thus, there is approximately a 1% deviation in hydrodynamic attributes as a result of these magnetic fields. Considering that this is at the time when the magnetic

fields are at some of their greatest values, it is indicative that there will never be much greater than 1% deviation as a result of the magnetic fields.

Clearly, it is possible that the magnitudes of the internally created magnetic fields at the time of peak particle production are large enough to cause the trajectories of highly energetic particles to bend by as much as a few tenths of a millimeter after they travel 20 cm from the field. To accurately determine how large the deflection is and what the effect on the distribution is, two things need to be done. First, there need to be self consistent calculations which take into account back current and convection. Second, there also needs to be a particle trajectory-tracking program that determines the amount of deflection as a function of angle of emission. Furthermore, this program would actually compute the yield for the changing magnetic fields. This work indicates that magnetic fields cannot be ruled out as the cause of this variation in particle yields around an imploding target.

6. Acknowledgments

I would like to thank Dr. R. S. Craxton for running the program, and allowing me to participate in this summer program. I would also like to thank Chris Piro, Matt Fiedler, and everyone else who has helped me with my project and presentation. Most of all, I would like to thank my advisor, Dr. Radha Bahukutumbi for assisting, teaching and mentoring me.

7. Appendix A: Equations

Variables And Constants:

n_e: electron density

e: elementary charge of an electron

E: electric field strength

k: Boltzmann constant

t_e: electron temperature

c: light speed

B: magnetic field strength

v: the velocity of the fluid

l: the length scale for the field

r: the radial coordinates of a cell in the simulation

θ: the polar coordinate of a cell in the simulation

The formula for the electric field in terms of the electron pressure gradient:

$$n_e eE = \nabla\left(n_e k t_e\right)$$

Faraday's Law; the law which gives the time dependent partial derivative of magnetic field strength as a function of the curl of electric field strength:

$$\nabla \times E = \frac{-1}{c}\frac{\partial B}{\partial t}$$

The formula used to calculate the time dependent partial derivative of the magnetic field as a function of the cross product of the gradients of electron temperature and density; this formula is a combination of the electrical field formula and Faraday's law:

$$\frac{\partial B}{\partial t} = \frac{ck}{en_e}\nabla n_e \times \nabla t_e$$

These gradients were computed numerically by taking a Taylor series approximation of the differences in values of t_e and n_e over a set of cells, around one cell a, in the radial and polar directions, yielding:

$$\frac{\partial t_e}{\partial r}(a) = \frac{1}{\Delta r_{31}\Delta\theta_{42} - \Delta r_{42}\Delta\theta_{31}}\left(\left(\Delta\theta_{42}t_{e3} + \Delta r_{42}t_{e1}\right) - \left(\Delta\theta_{42}t_{e1} + \Delta r_{31}t_{e3}\right)\right)$$

$$\frac{\partial t_e}{\partial \theta}(a) = \frac{1}{\Delta r_{31}\Delta\theta_{42} - \Delta r_{42}\Delta\theta_{31}}\left(\left(\Delta r_{31}t_{e4} + \Delta\theta_{31}t_{e2}\right) - \left(\Delta\theta_{42}t_{e2} + \Delta r_{31}t_{e4}\right)\right)$$

$$\frac{\partial n_e}{\partial r}(a) = \frac{1}{\Delta r_{31}\Delta\theta_{42} - \Delta r_{42}\Delta\theta_{31}}\left(\left(\Delta\theta_{42}n_{e3} + \Delta r_{42}n_{e1}\right) - \left(\Delta\theta_{42}n_{e1} + \Delta r_{31}n_{e3}\right)\right)$$

$$\frac{\partial n_e}{\partial \theta}(a) = \frac{1}{\Delta r_{31}\Delta\theta_{42} - \Delta r_{42}\Delta\theta_{31}}\left(\left(\Delta r_{31}n_{e4} + \Delta\theta_{31}n_{e2}\right) - \left(\Delta\theta_{42}n_{e2} + \Delta r_{31}n_{e4}\right)\right)$$

Here the subscripts correspond to the values of r, θ, n_e, and t_e at the four cells neighboring a. From here we can express our gradients in terms of these partial derivatives.

The formula for the time scale of integration (a sensitivity analysis for the scale length was incorporated into the deflection calculation):

$$\frac{l}{v} \approx \frac{10\mu m}{3\times 10^7 \frac{cm}{s}} = 30 ps$$

Calculations of Trajectory Bending

As long as a moving, charged particle is acted on by a magnetic field it will bend along a circular path. The radius of this circle is given by:

$$r = \frac{mv}{qB}.$$

where m, v, and q are the particle's mass, velocity and charge respectively, and B is the magnetic field's magnitude. We know the values of m, v, and q for different particles, so using trigonometry, we can compute the amount of deflection when the particles reach the detector, which is a distance of 20 cm, as a function of r and d, the distance over which the field acts on the particle.

8. Appendix B: Figures

Figure 1: This graph shows particle yield as a function of the placement of the detector. There are statistically significant differences between yield at different placements; KO-1 and TIM-5 for example.

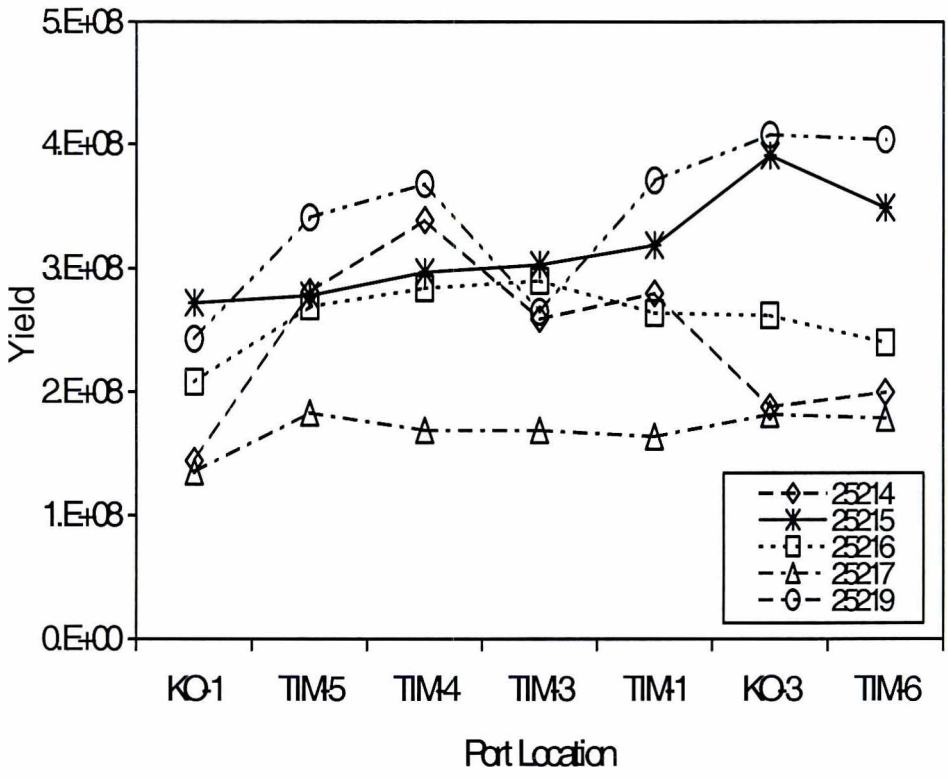

Figure 2: This contour plot shows the electron density in the imploding target at the time of peak particle production (about 1.9 ns). Notice the two "layers" of the graph. The sharp change between these layers represents the fuel shell surface. The irregularities in this interface are caused by the nonuniformities in the laser that are modeled in the DRACO simulation.

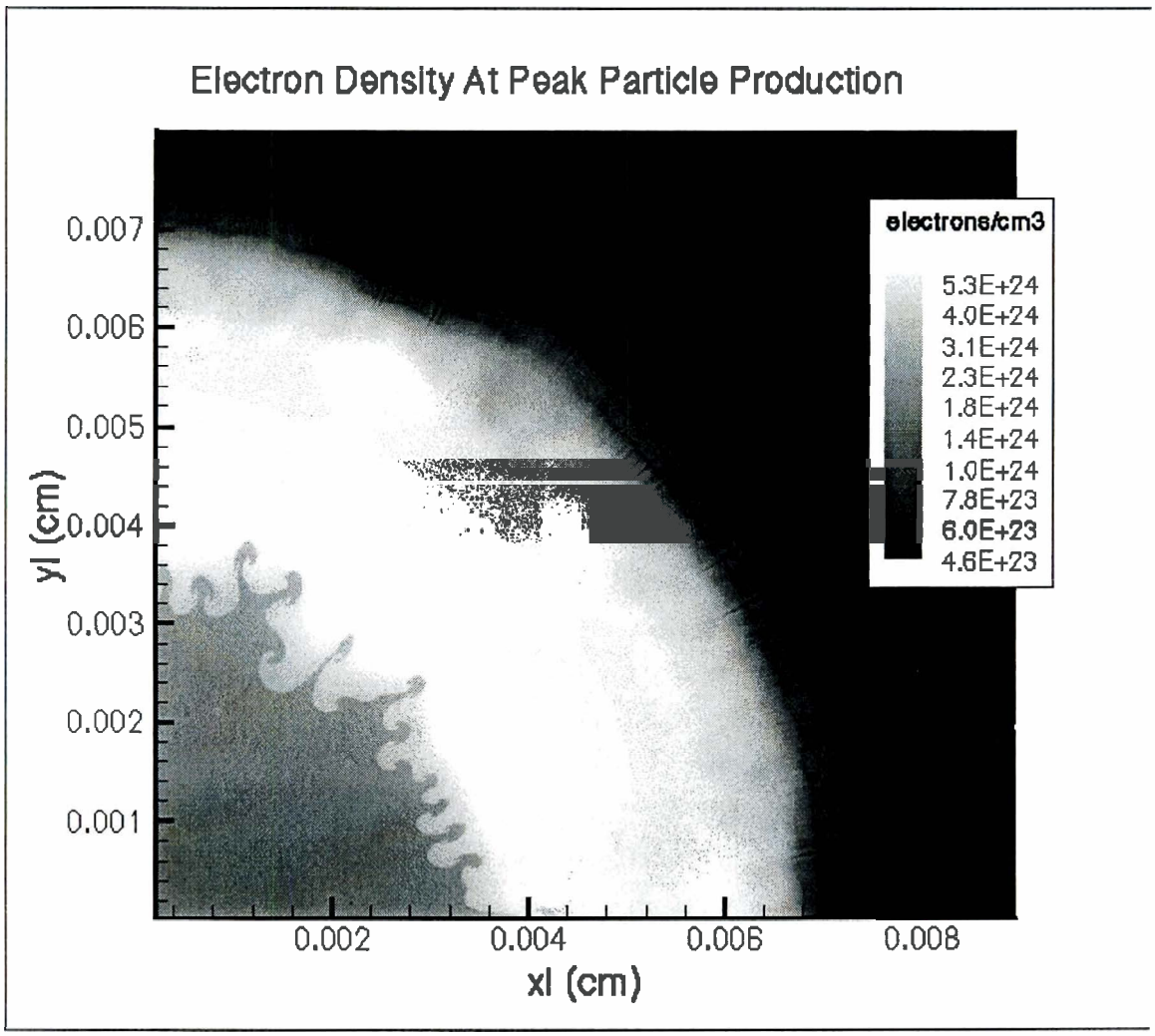

Figure 3: This contour plot shows electron temperatures in the imploding target at the time of peak particle production.

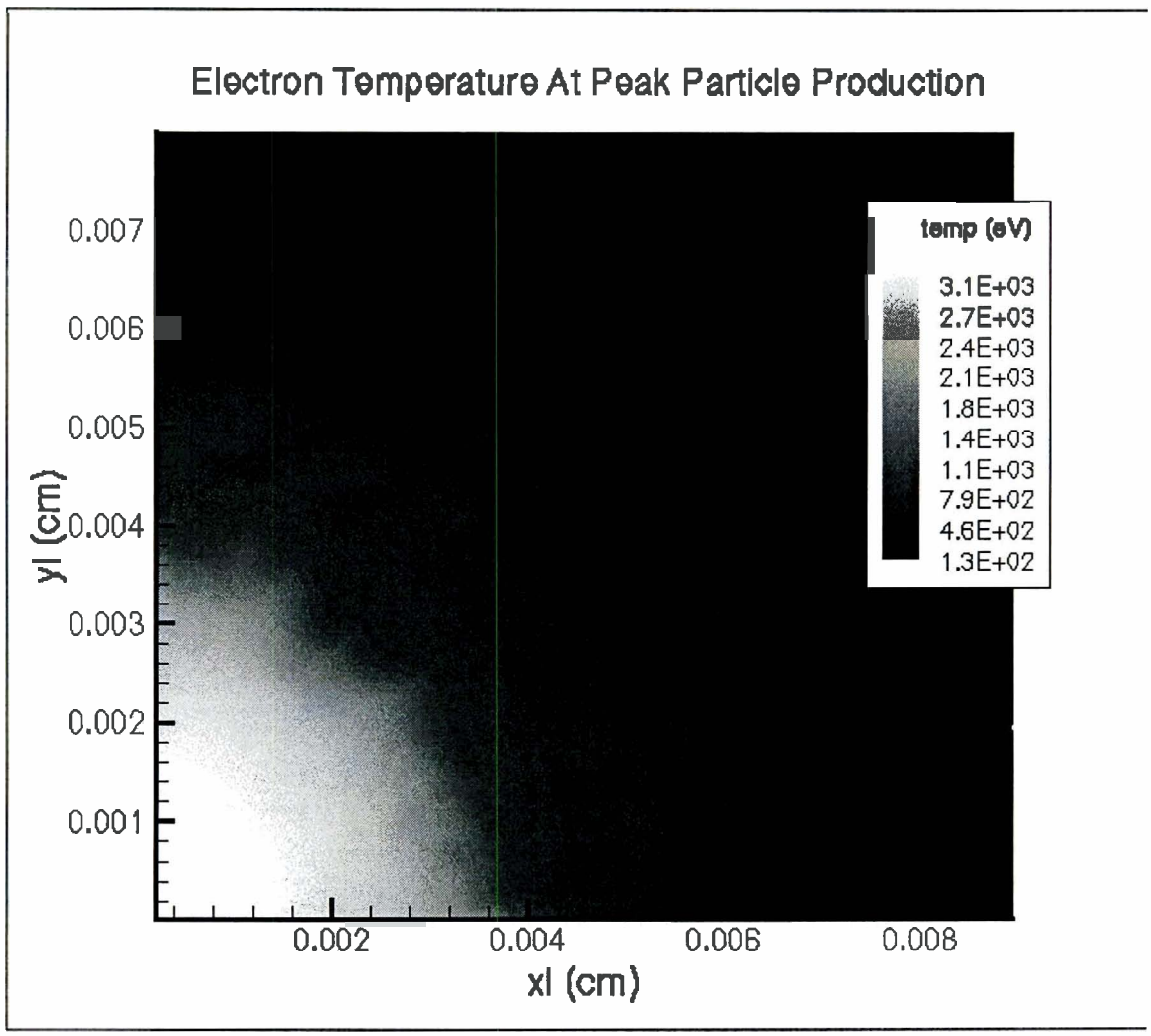

Figure 4: This diagram shows the vector gradients of the electron temperature at the time of peak particle production. Notice that the vectors at the fuel shell surface are orders of magnitude larger than those farther away. Also notice that the nonuniformities imprinted on the surface by the laser have led to gradients which do not follow a nice flow.

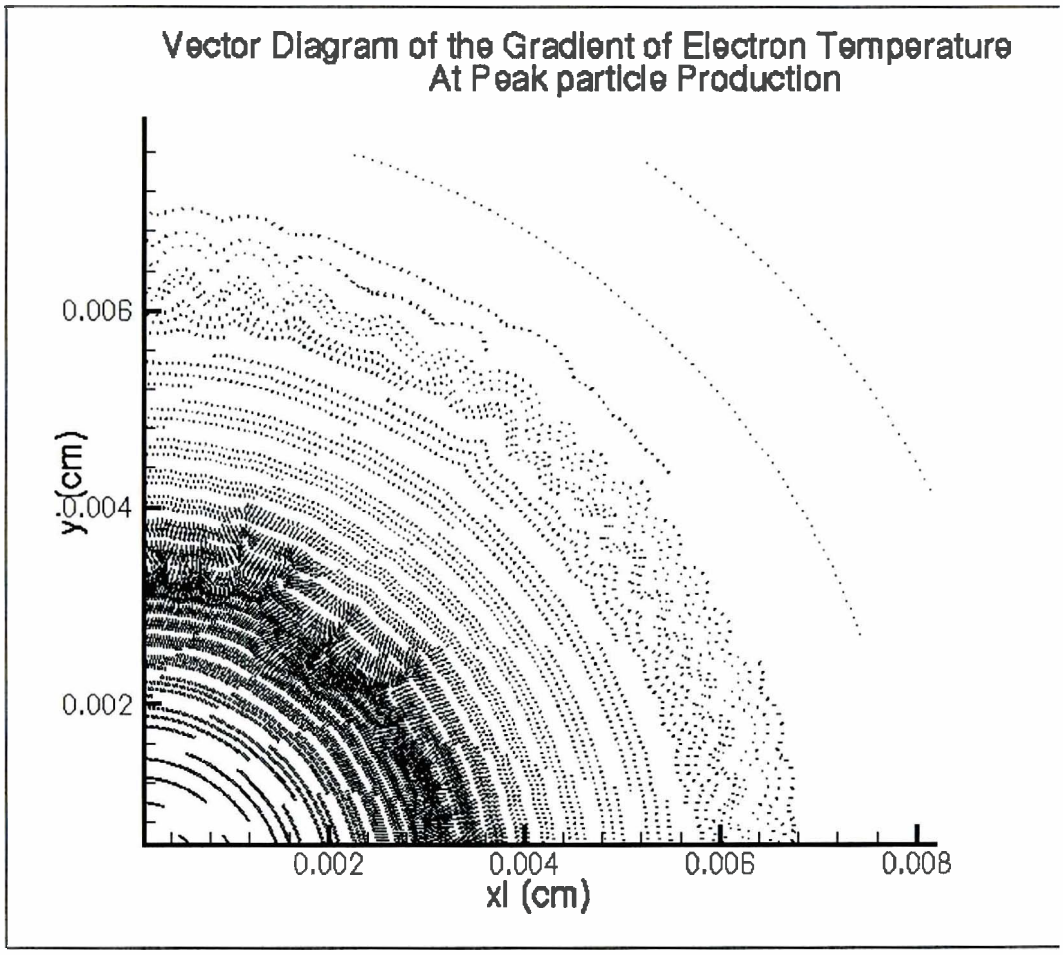

Figure 5: This diagram shows the vector gradients of the electron density at the time of peak particle production. Notice that while the vectors at the fuel shell surface are somewhat larger than those farther away, there is more uniformity here both in magnitude and direction of the vectors.

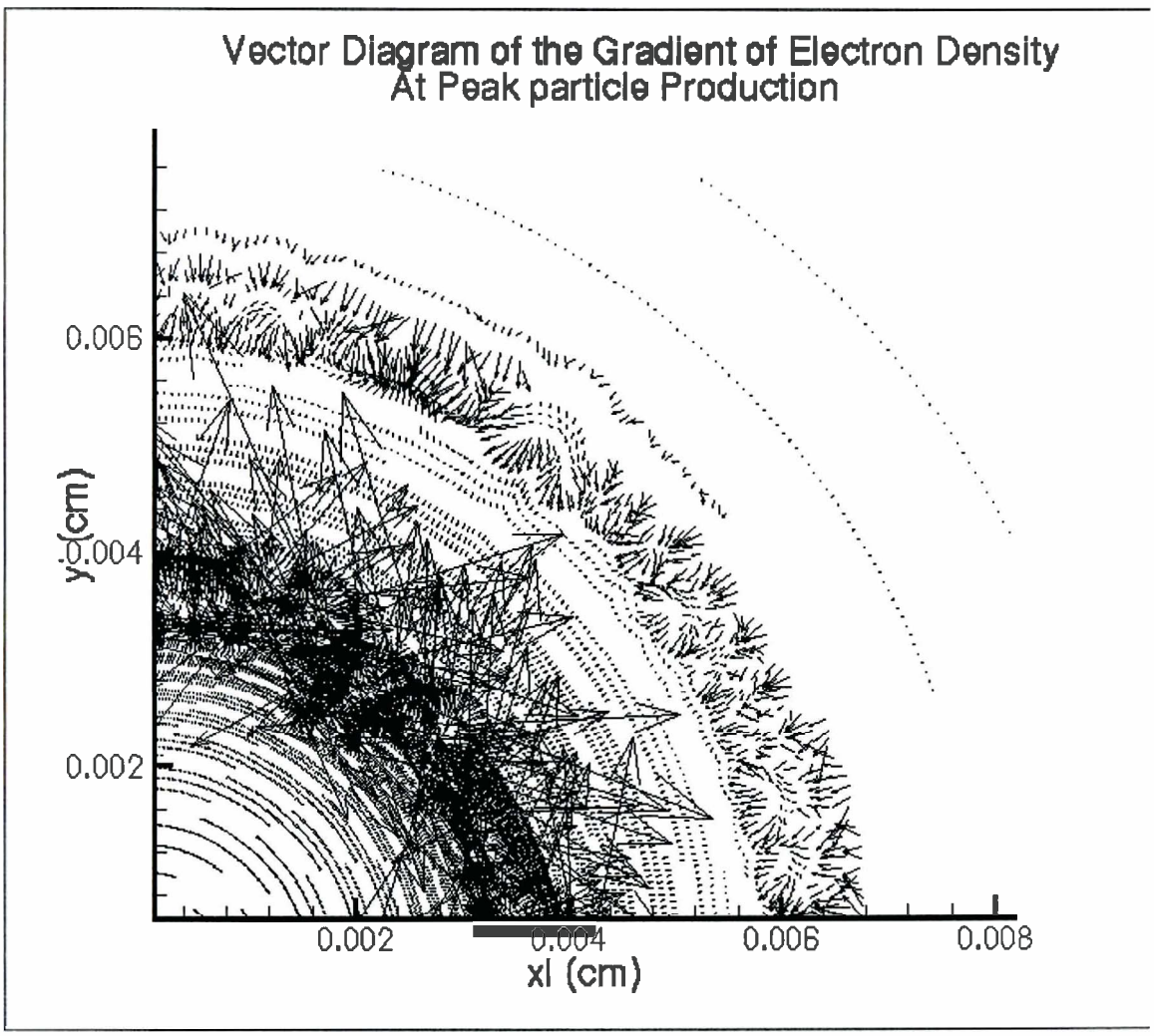

Figure 6: This contour plot shows the partial time derivative of magnetic field strength at the time of peak particle production.

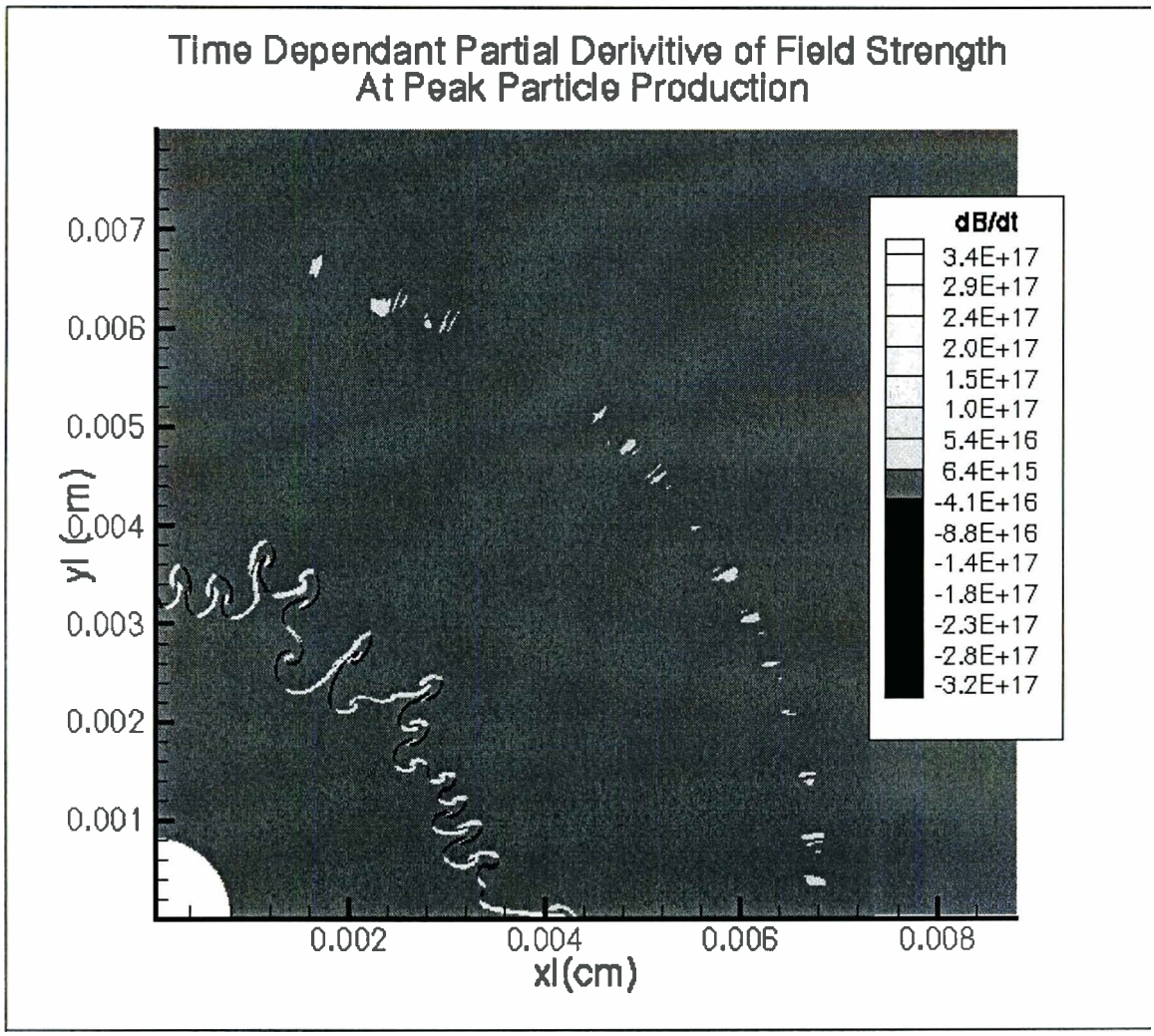

Figure 7: This contour plot shows the value of the magnetic field strength in the target at the time of peak particle production. Notice that the fields are (relatively) small except near the fuel shell interface where they are immense.

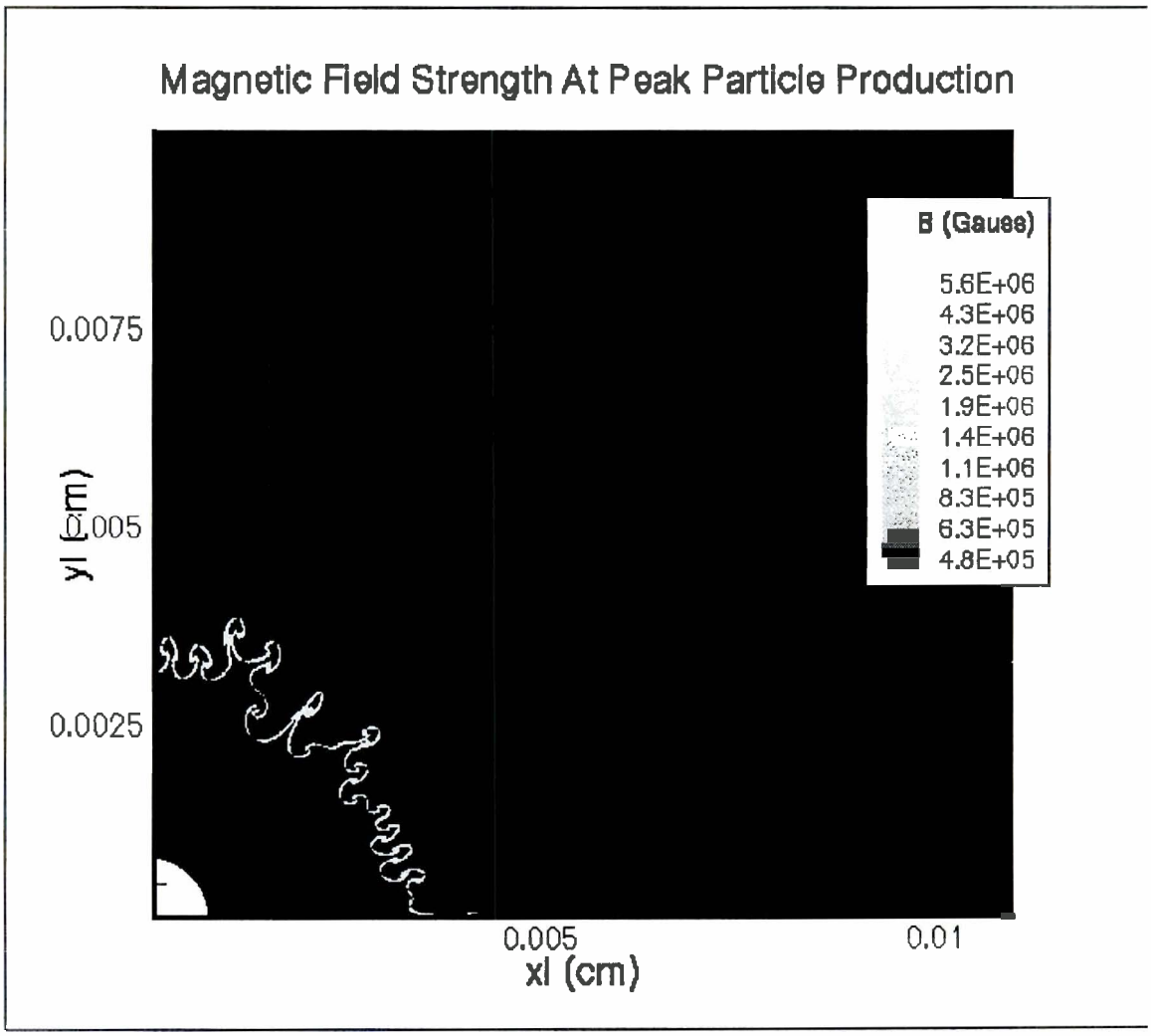

Figure 8: This contour plot shows the "scale length" for density gradients, or the approximate distance over which particles are subjected to magnetic fields caused by density gradients.

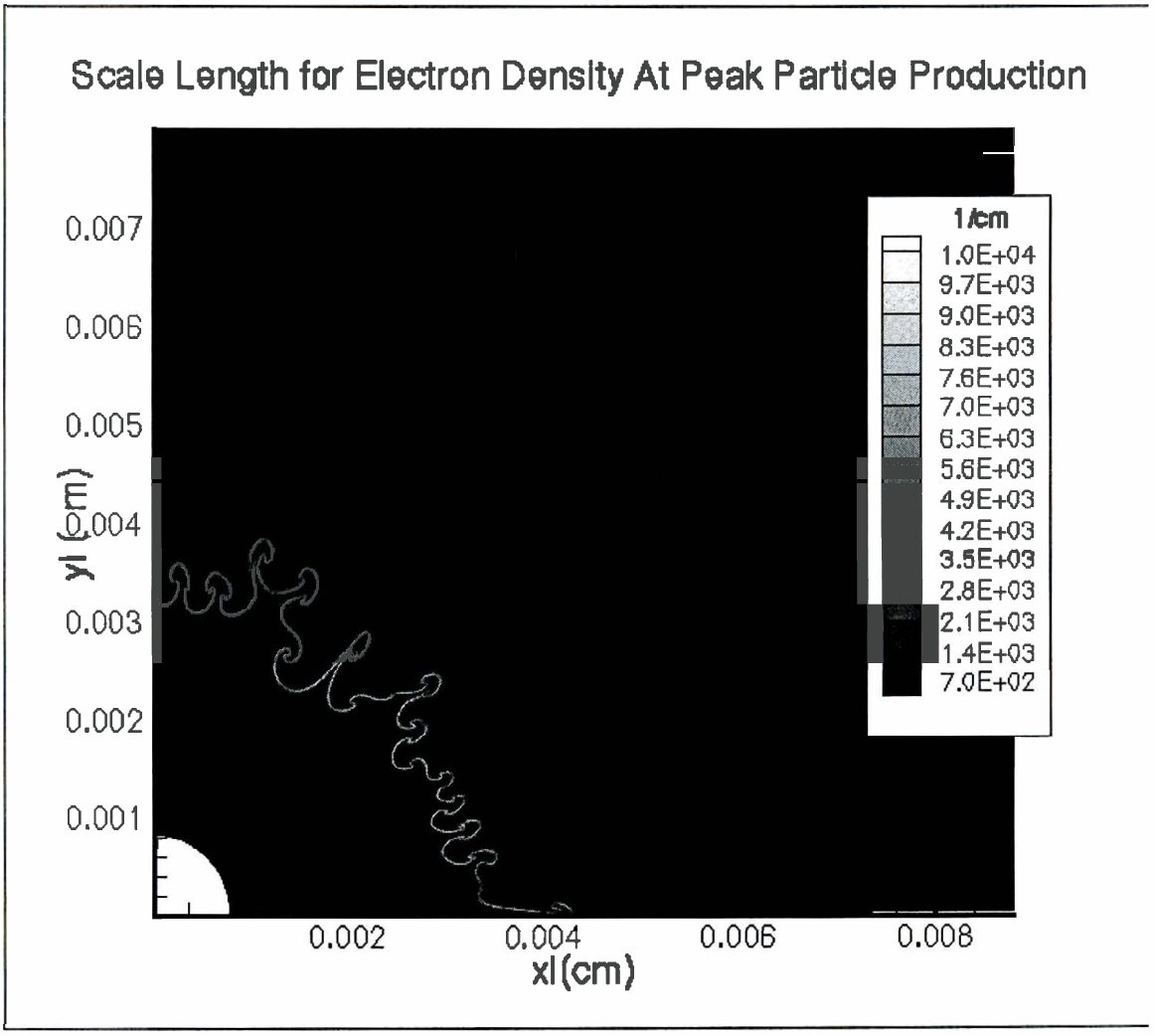

Figure 9: This contour plot shows the "scale length" for temperature gradients, or the approximate distance over which particles are subjected to magnetic fields caused by temperature gradients. Notice that the temperature change is gradual compared to the "quick" changes in density across the shell interface, so the scale lengths for temperature gradients are larger than those of density gradients.

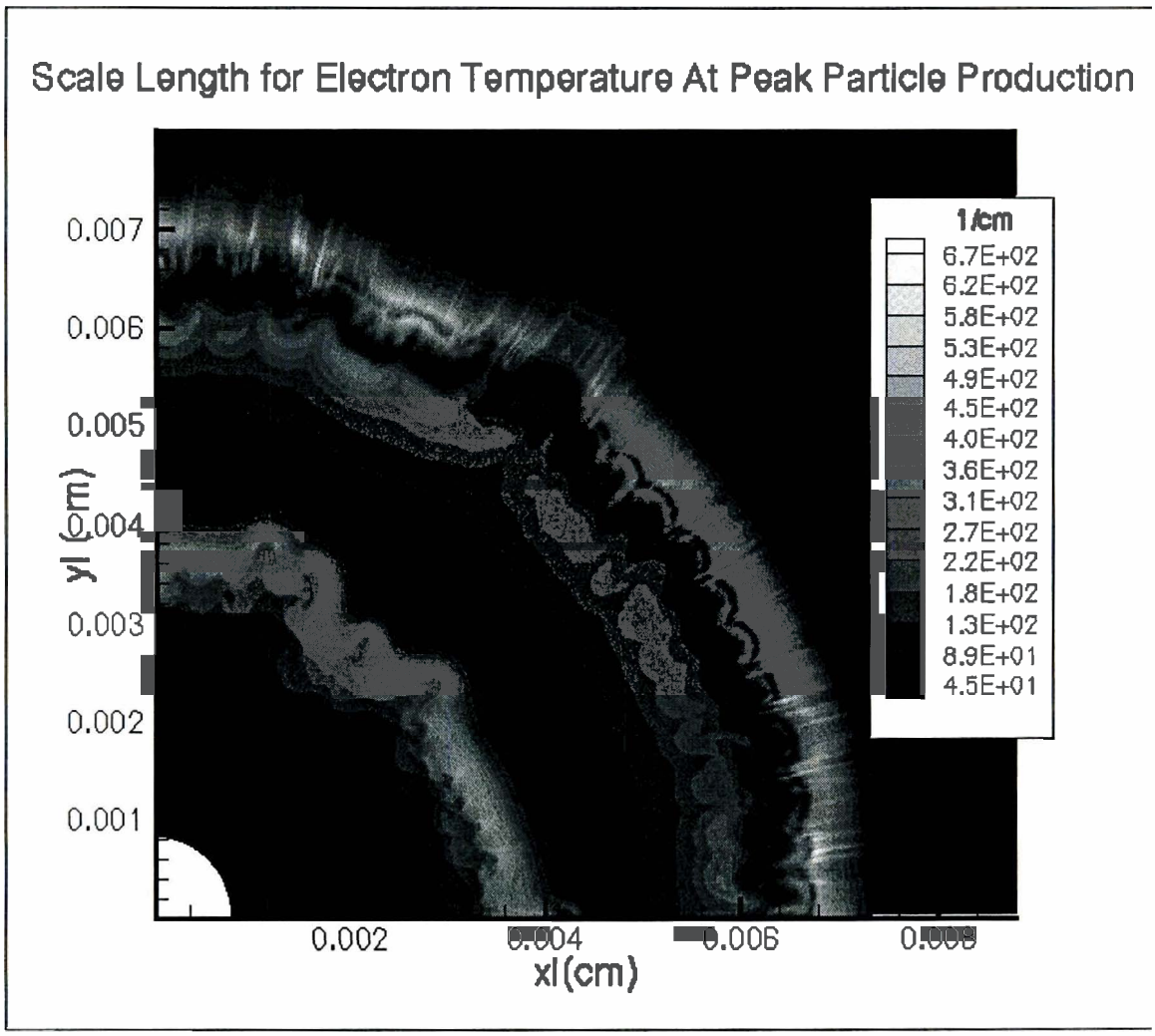

Figure 10: This contour plot shows the deflection for 14.5 MeV protons as a function of magnetic field strength and scale length. Particles in these implosions are subject to fields of magnitudes between 500 KiloGauss and 5 MegaGauss, over distances of between 2 and 4 microns, so that section of the graph has been highlighted.

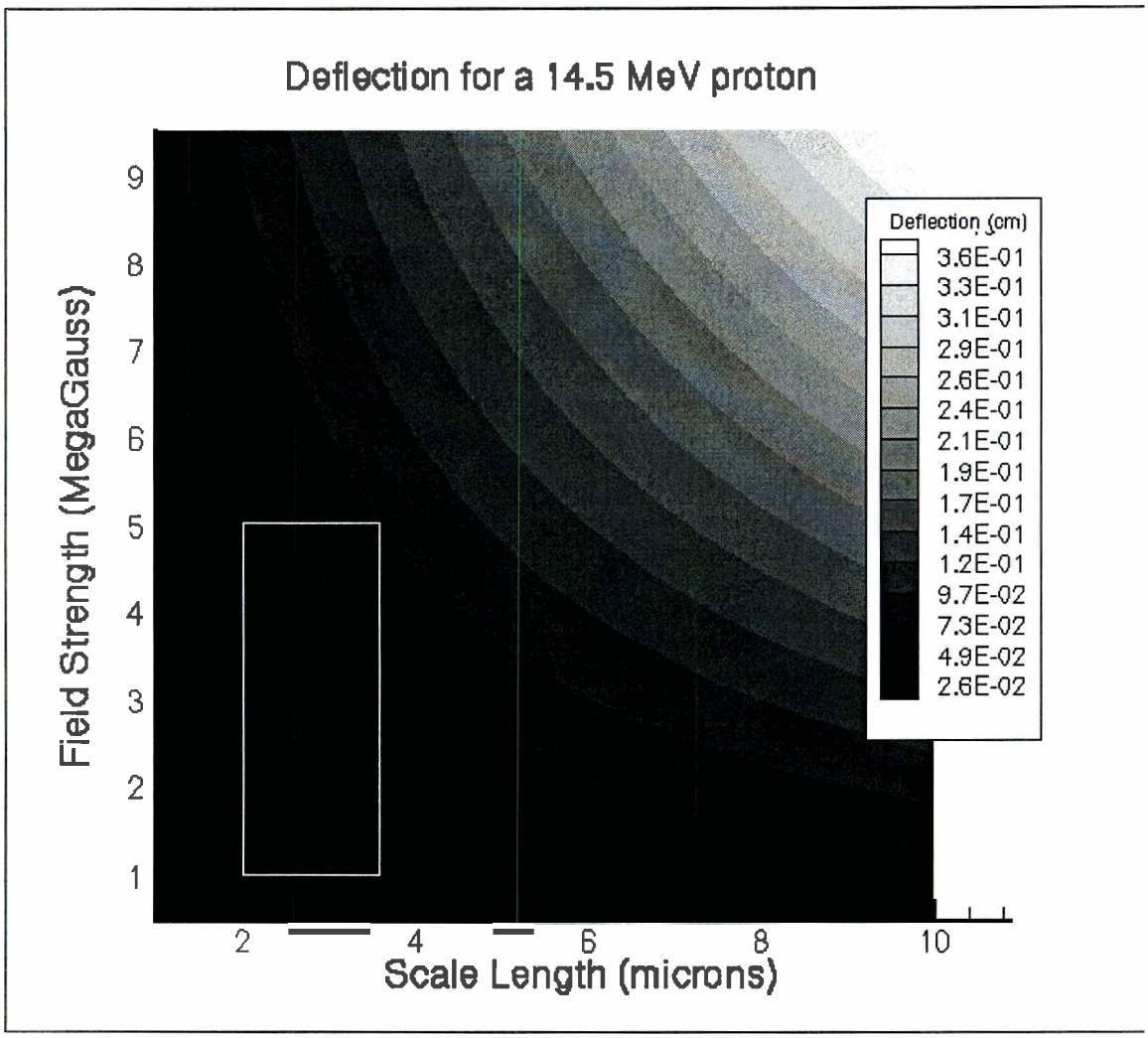

Figure 11: This contour plot shows the deflection for 10 MeV deuterons as a function of magnetic field strength and scale length. Particles in these implosions are subject to fields of magnitudes between 500 KiloGauss and 5 MegaGauss, over distances of between 2 and 4 microns, so that section of the graph has been highlighted.